Upwelling response to coastal wind profiles

X. J. Capet, P. Marchesiello, and J. C. McWilliams
Institute of Geophysics and Planetary Physics, University of California, Los Angeles, California, USA

Received 30 March 2004; accepted 25 May 2004; published 9 July 2004.

[1] The spatial structure of nearshore wind, as measured by aircraft and analyzed in high-resolution atmospheric models (e.g., COAMPS), has strong influence on the patterns of upwelling circulation, surface temperature, and biogeochemical processes in coastal regions. Using a regional oceanic model for both the Southern California Bight and the Central California Coast, we demonstrate the nature of this upwelling sensitivity and infer that present wind analyses do not adequately determine the most important wind properties, viz., the strength of the nearshore curl and the speed drop-off near the coast. *INDEX TERMS:* 4516 Oceanography: Physical: Eastern boundary currents; 3329 Meteorology and Atmospheric Dynamics: Mesoscale meteorology; 4279 Oceanography: General: Upwelling and convergences; 4255 Oceanography: General: Numerical modeling; 4247 Oceanography: General: Marine meteorology. **Citation:** Capet, X. J., P. Marchesiello, and J. C. McWilliams (2004), Upwelling response to coastal wind profiles, *Geophys. Res. Lett.*, *31*, L13311, doi:10.1029/2004GL020123.

1. Introduction

[2] Many coastal currents are forced by local wind stress. Oceanic models often have used wind analyses from large-scale climatologies or weather forecast models. But it is becoming more common to use special regional mesoscale wind analyses to improve modeled currents that are generally sensitive to small-scale wind features [*He et al.*, 2004; *Gan et al.*, 2004]. Off the Central California Coast (CCC) where the dominant alongshore winds favor upwelling circulation, the numerous capes and mountain ranges induce local wind anomalies (sometimes called expansion fans [*Winant et al.*, 1988]), and these are at least qualitatively captured in mesoscale atmospheric models. This is true for COAMPS [*Kindle et al.*, 2002] at high horizontal resolution (27 and 9 km) with expansion fans off the main capes (e.g., Blanco, Mendocino, Arena, and Conception). The intense stress curls associated with these orographic wind patterns induce a realistic response, e.g., the alongshore currents [*Marchesiello et al.*, 2003; *Di Lorenzo*, 2003]. COAMPS winds off the CCC also typically exhibit a transition in the alongshore wind speed within a narrow coastal strip where the wind stress decreases to about 10–20% of its offshore value (Figure 1). The physical cause of this drop-off is the land-sea change in the surface drag and boundary layer, which are delicate atmospheric modeling issues. The validations of COAMPS by *Kindle et al.* [2002] and *Pickett and Paduan* [2003] only marginally address this wind pattern issue because of sparseness of time-averaged wind measurements so close to the shore. The atypical availability of COAMPS winds at resolutions of 27, 9, and 3 km during August 2003 allows a better look at resolution sensitivity. The corresponding cross-shore profiles of alongshore wind stress averaged over the Pt. Sur region (Figure 1) all exhibit an expansion fan (i.e., the offshore extremum) and nearshore drop-off, but their structures differ significantly with the resolution. Most notably, the drop-off takes place over an increasingly small region as the resolution increases and wind curl increases proportionally, indicating that the true structure is indeterminate by current modeling practices. *Chao et al.* [2003] have developed a procedure that blends COAMPS winds with QuikSCAT scatterometer analyses (QCT). The blended wind (BLD) is an improvement in accuracy over either COAMPS or QCT alone. However, the scatterometer analyses are not reliable within ~50 km of the coastline, so the BLD winds rely on COAMPS nearshore and inherit its profile uncertainty.

[3] Since there is no consensus on the nearshore wind profile and the issue may not be resolvable without new measurements, we present here an assessment of how the wind profile affects the upwelling circulation and associated temperature structure (and, by implication, the biogeochemical consequences). Upwelling can result from both a coastal divergence of the seaward Ekman current (forced by alongshore stress at the coast) and an upward Ekman pumping associated with cyclonic stress curl (forced by nearshore wind drop-off), we expect COAMPS-like winds to favor the latter mechanism and be detrimental to the former. Using a simple Ekman current model and wind estimates from COAMPS or the CODE and SMILE experiments, *Pickett and Paduan* [2003] and *Enriquez and Friehe* [1995] argued that the upward Ekman pumping associated with a large curl is comparable in magnitude with the effect of Ekman coastal divergence, and that the net upwelling might be independent of the separate contributions since increased Ekman pumping would compensate for any decrease in coastal divergence.

[4] In our model solutions we show that the uncertainties in the transition scale and magnitude for the drop-off strongly affect coastal currents and temperature. During a conspicuously strong upwelling event in the Southern

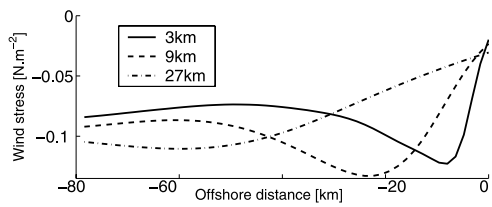

Figure 1. COAMPS alongshore wind stress vs. distance to the coast at 3 different resolutions. The wind is averaged over a 30 km alongshore interval south of Pt. Sur during August 2003.

0094-8276/04/2004GL020123

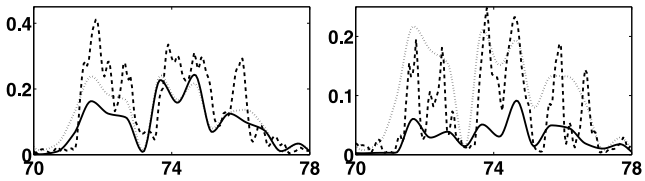

Figure 2. Wind stress (in Nm^{-2}) series at the NOAA (left, 33°44′42″N, 119°05′02″W) and UCLA moorings (right, 33°55′900″N, 118°42′937″W) during part of March 2002 (the x-axis gives the time in days elapsed since January 1, 2002). Mooring data (dashed line), BLD (solid line) and modified BLD (dotted line) are represented. Mooring data have been low-passed filtered to remove the high frequencies absent in the twice-daily blended wind.

California Bight (SCB), nearshore wind forcing sensitivities control the agreement between solutions and observations (Section 3). Off the CCC with its prevalent upwelling conditions, we show that nearshore wind drop-off diminishes upwelling; i.e., the hypothesized compensation between nearshore Ekman transport and upward Ekman pumping does not fully occur.

2. Numerical Model and Configurations

[5] Our numerical model is ROMS [*Shchepetkin and McWilliams*, 2004] with adaptive open boundary conditions and an online, down-scaling, grid nesting capability (P. Penven et al., Application of the ROMS embedding procedure to the central California upwelling system, submitted to Ocean Modelling, 2004). In both solutions reported here, we use 3 grid levels (denoted by L1, L2, and L3) to allow the local currents to evolve under the influence of the regional circulation as well as the local wind forcing. L1 encompasses the California Current System (CCS) at a low horizontal resolution of 15–20 km. L2 and L3 have grid sizes of 5–6 km and 1.5–2 km, respectively. In the south (Section 3), L2 spans the SCB, and L3 contains Santa Monica Bay. In the north (Section 4), L2 spans the CCC, and L3 contains Monterey Bay. In the vertical, 20 σ-coordinate levels are unevenly distributed for good resolution of the upper ocean. In both cases, we compare the intensity of the upwelling induced by two winds differing by the magnitude of the drop-off at the coast (BLD at 27 km resolution versus a modified version of it in Section 3; BLD at 9 km resolution versus QuikSCAT for Section 4).

3. An SCB Event

[6] In March 2002 a major upwelling event took place in the SCB in response to southeastward winds (i.e., parallel to the coast) with an average stress around 0.2 Nm^{-2} between days 71 and 76 (Figure 2). The upwelling response is clearly visible in the Sea Surface Temperature (SST) immediately after the event when cold water has invaded much of the nearshore region (Figure 3 (left)). This event had major environmental consequences due to a bloom of toxic algae that sickened sea lions and other species. We calculated model solutions using the BLD winds available for this period (27 km resolution). The upwelling produced by the model and associated SST anomaly are notably weak compared to the observations (Figure 3).

[7] Based on comparisons between NOAA and UCLA moored wind measurements (Figure 2) and the COAMPS winds, a possible explanation for this discrepancy is the weakness of the nearshore wind in COAMPS. At the NOAA mooring, both the direction and wind intensity are rather close to the observations. Nearer shore at the UCLA mooring, the wind direction is still correct but its intensity is 3 to 4 times smaller than the observed wind during this period. Therefore, a new solution was calculated using a version of the COAMPS winds modified in a nearshore strip 30 km wide (Figure 2), in which the relative drop-off was made spatially uniform and equal to the one observed between the NOAA and UCLA moorings. In the absence of more complete wind measurements, we view this modification as a way to assess the uncertainty in our solutions.

[8] With this modified wind the SST near the coast reaches 11°C (2°C colder than without the modification), in good agreement with the observed SST. This shows that the nearshore wind profile has a strong influence for the upwelling and that its uncertainty in the wind stress value at the coast is an important issue for model veracity.

4. Recurrent Upwelling off Pt. Sur

[9] Having demonstrated nearshore wind sensitivity for a particular event, we further examine it for the recurrent upwelling off the CCC. The wind in this region is upwelling-favorable almost year round (Figure 4), so the upwelling structure and circulation can be analyzed with long-term averaging. Two solutions are calculated using different mean-monthly wind climatologies. (Other solutions with synoptic winds indicate only a minor influence on the average state of the CCS, including its coastal upwelling.) The model is spun up for three years, starting from Levitus; the next two years are analyzed for the climatological circulation within the L3 domain.

[10] These solutions (denoted by $\mathcal{QCT}$ and $\mathcal{BLD}$) are forced with QCT (with the coastal gap filled by an objective analysis yielding a smooth profile toward the coast with weak drop-off) or BLD winds. Since both wind fields are

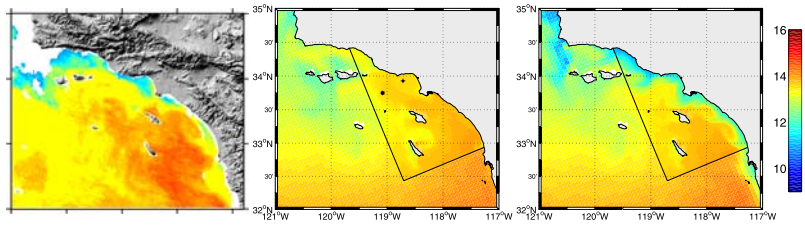

Figure 3. SST (°C) in the Bight on March 20 (year day 79): observed (left) and modeled with $\mathcal{BLD}$ winds, either modified (right) or not (middle). The * and + symbols in the middle panel indicate the location of the NOAA and UCLA moorings.

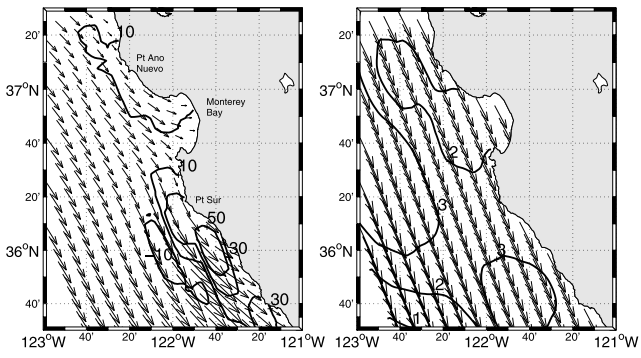

Figure 4. Summer-mean central California wind stress (arrows; the maximal value is 0.146 Nm^{-2}) and curl (isolines, in Pa/100 km) for both $\mathcal{BLD}$ (left) and $\mathcal{QCT}$ (right).

similar everywhere except nearshore [*Chao et al.*, 2003] (see also Figure 4) comparison of $\mathcal{QCT}$ and $\mathcal{BLD}$ allows us to assess the effects of nearshore scales present in BLD. Note the wind intensification off Pt. Sur and the sharp alongshore wind drop-off and curl increase nearshore in the BLD winds in the summer-mean (Figure 4).

[11] At the large scale (i.e., in L1 and L2), both solutions have a realistic state for the CCS [*Marchesiello et al.*, 2003] with modest sea level and current differences. At the smallest scale (L3), the solutions are highly turbulent with intense sub-mesoscale activity. The upwelling brings cold water (~11°C) to the surface broadly in this region, with active centers off Pt. Sur and Año Nuevo. Model/data comparisons (e.g., using temperature measured along CalCOFI line 67) are inconclusive as to which solution is closer to the observations: we found discrepancies of up to one degree for both solutions although the patterns differ. Therefore, we limit our discussion to the wind sensitivity and do not judge their respective skills (both have deficiencies nearshore, by construction for QCT and in Figure 1 for COAMPS).

[12] The summer-mean temperatures (Figure 5) and vertical velocity (not shown) in cross-shore sections south of

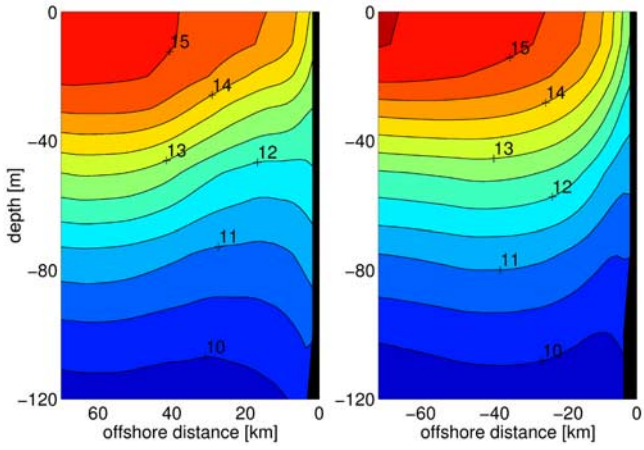

Figure 5. Cross sections off Pt. Sur of temperature (°C), alongshore velocity (middle; cm s^{-1}) averaged over the summer season and 30 km alongshore. The model is forced with either $\mathcal{BLD}$ (left) or $\mathcal{QCT}$ (right) winds.

Table 1. Number of Upwelling Parcels Released at Depth $d1$ That Ascend to Depth $d2$ Within 15 Days[a]

d1 → d2	$N^{\mathcal{QCT}}_{d1\to d2}$	$N^{\mathcal{BLD}}_{d1\to d2}$	$R_{d1\to d2}$
100 m → 70 m	2869	1951	0.68
100 m → 50 m	1359	571	0.42
50 m → 35 m	4753	3829	0.80
50 m → 20 m	3139	1632	0.52
50 m → 10 m	2354	1036	0.44

[a]The middle columns list the numbers for $\mathcal{QCT}$ (left) and $\mathcal{BLD}$ (right) winds, and the final column is their ratio.

Pt. Sur — where the QCT and BLD winds differ significantly — suggest that the coastal divergence (associated with seaward Ekman transport) and Ekman pumping upwelling mechanisms lead to different upwelling structures. Coastal SST is 1°C colder in $\mathcal{QCT}$ than in $\mathcal{BLD}$. The 12°C isotherm reaches 25m depth in $\mathcal{QCT}$ compared to only 50 m in $\mathcal{BLD}$. More generally, the thermocline rises sharply at the coast in $\mathcal{QCT}$, indicating that most of the upwelling is concentrated where coastal divergence occurs. On the other hand, $\mathcal{BLD}$ exhibits a more gradual rise and broad doming in the strip 10–30 km off the coast. The location of the doming is consistent with the wind stress curl maximum. Vertical velocities are in agreement with these temperature fields. Nearshore (0–10 km from the coast) upward vertical velocities are more marked in $\mathcal{QCT}$: the area occupied by velocities over 5 m/day (in the 2D cross section plane) is 40% larger in $\mathcal{QCT}$ relative to $\mathcal{BLD}$. On the other hand, BLD exhibits a secondary core of upward velocities 15 to 30 km from the shore that extends below the thermocline (3 m/day at 70 m depth).

[13] We also calculate Lagrangian diagnostics to quantify the upward displacements between two given depths, without any subgrid mixing nor surface heat flux influences (implicitly present when comparing temperatures) and separate from any subsequent downward displacements. This is a more relevant measure of upwelling from the biological perspective of nutrient input to the euphotic zone. Parcels are released at 2 depths (100 and 50 m) and 7 times (every 5 days between July 1 and 31). The releases horizontally span the L3 subdomain with a spacing of 5 km. This implies over 9000 parcels per release depth. Parcel trajectories are computed online with a 4th-order time stepping scheme and trilinear spatial interpolation. No parameterization of subgrid-scale mixing is applied to the parcels (no random walking). The parcels' fate is summarized in Table 1 as the number of parcels ($N^{\mathcal{QCT}}_{d1\to d2}$ for $\mathcal{QCT}$ and $N^{\mathcal{BLD}}_{d1\to d2}$ for $\mathcal{BLD}$) starting from depth $d1$ and reaching a higher level $d2$, as well as their ratio $R_{d1\to d2} = N^{\mathcal{BLD}}_{d1\to d2}/N^{\mathcal{QCT}}_{d1\to d2}$. The upward displacement numbers are significantly greater in $\mathcal{QCT}$:

Table 2. Offshore Distribution of Upwelling Parcels for $\mathcal{QCT}$ and $\mathcal{BLD}$ Winds Partitioned Into Nearshore (0–10 km From the Coast), Adjacent (10–30 km), and Further Offshore Strips[a]

	$\mathcal{QCT}$		$\mathcal{BLD}$	
d1 → d2	0–10 km	10–30 km	0–10 km	10–30 km
100 → 70	1147 (0.40)	488 (0.17)	702 (0.36)	507 (0.26)
100 → 50	611 (0.45)	312 (0.23)	240 (0.42)	189 (0.33)
50 → 35	1759 (0.37)	618 (0.13)	1455 (0.38)	459 (0.12)
50 → 20	1193 (0.38)	408 (0.13)	685 (0.42)	196 (0.12)
50 → 10	895 (0.38)	330 (0.14)	445 (0.43)	104 (0.10)

[a]The number of parcels and the fraction of the total upwelled parcels (in parentheses) are listed for each depth interval, offshore strip, and winds.

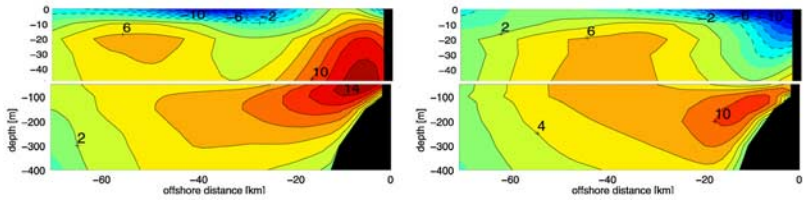

Figure 6. Same as Figure 5 for alongshore velocity (in cm s^{-1}). The interval between 2 isolines is 2 cm s^{-1}.

$R_{d1\rightarrow d2} < 0.8$ for any ($d1$, $d2$), especially for the largest vertical displacements (100 → 50 and 50 → 10. The offshore location where parcels are upwelled (i.e., their location when they reach $d2$) allows an assessment of the relative efficiency of coastal divergence and Ekman pumping (Table 2). For any choice of ($d1$, $d2$), around 40% of the upwelling occurs within 10 km from the coast, with no significant differences between $\mathcal{QCT}$ and $\mathcal{BLD}$. Upwelling occurring farther offshore (10–30 km; in the maximum wind curl) is smaller as it accounts for only 10 to 33% of the total upwelled parcels. However, deep upwelling (($d1$, $d2$) = (−100, −70) and (−100, −50)) in $\mathcal{BLD}$ is more evenly balanced between the coastal strips. The only place where $\mathcal{BLD}$ has more upwelled parcels than $\mathcal{QCT}$ is in the 10–30 km strip for ($d1$, $d2$) = (−100, −70).

[14] These Lagrangian diagnostics indicate that upwelling in the upper 100 m is primarily confined to nearshore and associated with coastal divergence, hence strongly dependent on the nearshore wind stress. The curl-induced Ekman pumping that results from the wind drop-off in BLD is not able to compensate for the lack of coastal divergence to achieve as high a level of upwelling overall.

5. Discussion

[15] The competition between coastal divergence and Ekman pumping explains how the nearshore wind profile affects the upwelling circulation. The occurrence of nearshore drop-off favors vertically and horizontally distributed upward Ekman pumping, while stronger nearshore winds (i.e., smaller drop-off) favor intense and localized coastal upwelling. The latter mechanism is therefore more efficient in raising deep parcels to near the surface.

[16] The wind structure close to the coast also plays an important role in determining the alongshore current structure [*Marchesiello et al.*, 2003]. Equatorward winds at the coast force a surface equatorward jet and poleward undercurrent. But the depth-averaged poleward currents are related to positive wind curl through Sverdrup balance (although the eddy Reynolds stress further acts to redistribute the wind-curl input). In $\mathcal{BLD}$ large positive wind curl and weak coastal wind favor poleward currents, and vice versa for $\mathcal{QCT}$. As a result, alongshore currents significantly differ between the two solutions (Figure 6); e.g., the $\mathcal{BLD}$ undercurrent almost surfaces at the shore, whereas it is confined below 40 m with weaker velocities in $\mathcal{QCT}$. Mesoscale eddy energy levels, even hundreds of kilometers offshore, and cross-shore eddy fluxes are also strongly affected. Important consequences on the ecosystem occur since upwelling and alongshore current sensitivities will affect nutrient supply as well as alongshore retention of organisms.

[17] High-resolution atmospheric models such as COAMPS represent a necessary step forward for coastal oceanic modeling since they contain mesoscale wind patterns that significantly influence nearshore circulation. However, based on the present results, we believe that these wind products need further improvement and validation for them to suffice as oceanic forcing fields. The facts that the COAMPS wind profile does not seem to converge as its resolution increases (Figure 1) and that some mooring measurements indicate it overestimates the nearshore wind drop-off are key issues for the upwelling response.

[18] **Acknowledgments.** The authors thank J. Doyle, Y. Chao and J. Kindle for making their wind products available. This research was supported by NOPP under grant (NAG13-00042) and by National Computational Science Alliance.

References

Chao, Y., Z. Li, J. Kindle, J. Paduan, and F. Chavez (2003), A high-resolution surface vector wind product for coastal oceans: Blending satellite scatterometer measurements with regional mesoscale atmospheric model simulations,*Geophys. Res. Lett.*, *30*(1), 1013, doi:10.1029/2002GL015729.

Di Lorenzo, E. (2003), Seasonal dynamics of the surface circulation in the Southern California Current System, *Deep Sea Res., Part II*, *50*, 2371–2388.

Enriquez, A. G., and C. Friehe (1995), Effects of wind stress and wind stress curl variability on coastal upwelling, *J. Phys. Oceanogr.*, *25*, 1651–1671.

Gan, J., J. S. Allen, and R. M. Samelson (2004), On open boundary conditions for a limited-area coastal model off Oregon. Part 2: Response to wind forcing from a regional mesoscale atmospheric model, *Ocean Modell.*, doi:10.1016/j.ocemod.2003.12.007, in press.

He, R., Y. Liu, and R. H. Weisberg (2004), Coastal ocean wind fields gauged against the performance of an ocean circulation model, *Geophys. Res. Lett.*, *31*, doi:10.1029/2003GL019261, in press.

Kindle, J. C., R. Hodur, S. deRada, J. Paduan, L. Rosenfeld, and F. Chavez (2002), A COAMPS reanalysis for the eastern Pacific: Properties of the diurnal sea breeze along the central California coast, *Geophys. Res. Lett.*, *29*(24), 2203, doi:10.1029/2002GL015566.

Marchesiello, P., J. C. McWilliams, and A. F. Shchepetkin (2003), Equilibrium structure and dynamics of the California Current system, *J. Phys. Oceanogr.*, *33*, 753–783.

Pickett, M. H., and J. D. Paduan (2003), Ekman transport and pumping in the California Current based on the U.S. Navy's high-resolution atmospheric model (COAMPS), *J. Geophys. Res.*, *108*(C10), 3327, doi:10.1029/2003JC001902.

Shchepetkin, A. F., and J. C. McWilliams (2004), The Regional Oceanic Modeling System: A split-explicit, free-surface, topography-following-coordinate oceanic model, *Ocean Modell.*, in press.

Winant, C. D., C. Dorman, C. Friehe, and R. Beardsley (1988), The marine layer off northern California: An example of supercritical channel flow, *J. Atmos. Sci.*, *45*, 3588–3605.

X. J. Capet, P. Marchesiello, and J. C. McWilliams, IGPP, UCLA, 405 Hilgard Avenue, Los Angeles, CA 90095-1567, USA. (capet@atmos.ucla.edu)